



100 MHz bandwidth planar laser-generated ultrasound source for hydrophone calibration

Srinath Rajagopal^{a,*}, Ben T. Cox^b

^a *Ultrasound and Underwater Acoustics Group, National Physical Laboratory, Hampton Road, Teddington TW11 0LW, UK*

^b *Department of Medical Physics and Biomedical Engineering, University College London, Malet Place Engineering Building, Gower Street, London WC1E 6BT, UK*

ARTICLE INFO

Keywords:

Hydrophone
Calibration
High-frequency
Deconvolution
Photoacoustics

ABSTRACT

High-frequency calibration of hydrophones is becoming increasingly important, both for clinical and scientific applications of ultrasound, and user safety. At present, the calibrations available routinely to the user community extend to 60 MHz. However, hydrophones that can measure beyond this are available, and ultrasonic fields often contain energy at higher frequencies, e.g., generated through nonlinear propagation of high-amplitude ultrasound used for therapeutic applications, and the increasing use of higher frequencies in imaging. Therefore, there is a need for calibrations up to at least 100 MHz, to allow ultrasonic fields to be accurately characterized, and the risk of harmful bioeffects to be properly assessed. Currently, sets of focused piezoelectric transducers are used to meet the pressure amplitude and bandwidth requirements of Primary Standard calibration facilities. However, when the frequency is high enough such that the size of the ultrasound focus becomes less than the hydrophone element's diameter, the uncertainty due to spatial averaging becomes significant, and can be as high as 20% at 100 MHz. As an alternate to piezoelectric transducers, a laser-generated ultrasound calibration source was designed, fabricated, and characterized. The source consists of an optically absorbing carbon-polymer nanocomposite excited by a large-diameter 1064 nm laser pulse of 2.6 ns duration. Peak pressure amplitudes of several Mega-Pascal were readily achievable, and the signal contained measurable frequency components up to 100 MHz. The variation in the pressure amplitudes was less than 2% from its mean over a three-hour test period. The ultrasound beam was sufficiently broad that the uncertainties due to spatial averaging were negligible.

1. Introduction

Ultrasound (US) can cause mechanical as well as thermal damage to biological tissue under certain excitation conditions [1,2]. When an US source is used for biomedical imaging or therapy it is therefore imperative that it is carefully characterized to ascertain its safety or efficacy. Frequencies used in biomedical applications range from a few hundreds of kHz to 100 MHz and higher. For example, frequencies under 1 MHz are used in low-intensity ultrasound neuromodulations [3], frequencies of the order of 1–15 MHz are used for clinical imaging, and 10–80 MHz range are applied in preclinical research [4]. The high amplitude (tens of MPa) of US waves used therapeutically in thermal ablation and lithotripsy propagate nonlinearly in water generating harmonic frequency components as high as 100 MHz [5]. The standard devices used to characterize the acoustic fields generated by medical ultrasound equipment are miniature hydrophones manufactured using the piezoelectric polymer polyvinylidene fluoride (PVDF) [6]. Recently, robust hydrophones based on PVDF, as well as Fabry–Pérot US sensors,

have been developed for the characterization of the high intensity fields used in therapeutic ultrasound [7–10]. For quantitatively accurate field characterization, these devices need to be calibrated over the full range of frequency components present in the fields being measured. This characterization is required to ensure patient safety [11], for performance validation and compliance [12,13], and to assist the development of new high-frequency ultrasound technologies [14–16].

The calibration of hydrophones is performed by National Measurement Institutes (NMIs) to a traceable standard. First, a primary calibration is performed on a reference hydrophone, and this hydrophone is used subsequently for secondary calibration procedures. The uncertainty in this secondary calibration will include the uncertainty in calibrating the reference hydrophone as well as the uncertainties inherent to the secondary method. Currently, the user hydrophone uncertainty for hydrophones calibrated at the UK's NMI, the National Physical Laboratory (NPL) is 6–22% over 1–60 MHz (95% coverage probability). The uncertainty is similar for Physikalisch-Technische Bundesanstalt (PTB), Germany's NMI, over the same frequency range.

* Corresponding author.

E-mail address: srinath.rajagopal@npl.co.uk (S. Rajagopal).

The uncertainty at 100 MHz in their magnitude sensitivity using the primary method is at least 40% (95% coverage probability) [17]. There is therefore a need to reduce the uncertainty on the Primary Standard to as low as possible.

The primary methods (or standards) currently in use are based either on reciprocity or optical interferometry [18]. In both methods, the essential task is knowing what the acoustic field is at the position of the active sensing region of the hydrophone. In the reciprocity method, a transmit-receive transducer is used with a reflector placed at half the transducer-hydrophone separation corresponding to one and half times the near-field distance, and the acoustic field at the hydrophone position (in the absence of the reflector) can be inferred. This method is limited to frequencies below about 20 MHz for several reasons [19]. First, the transducer has a limited bandwidth on both transmission and reception; second, the alignment capability on the transducer must be very precise at shorter wavelengths because of the steep directionality of the transducer; third, the measurement method is limited to linear acoustic fields only, which means the measurement procedure will need to be repeated at every frequency of interest.

An alternative method is to use a two-stage substitution approach. Here, an acoustic field is first measured directly with an optical interferometer that can be traced directly to the optical wavelength used, and then the hydrophone being calibrated is placed in the known field [17,20–23]. This has three advantages: 1) displacement or velocity sensing interferometers (vibrometers) can measure over a wide frequency range, 2) the temporal and spatial characteristics of the acoustic field used in the calibration can be chosen to reduce the uncertainty in the measurements and 3) it is not restricted to the transmit bandwidth of the transducers. The frequency range is limited by two factors: the signal-to-noise ratio (SNR), which will depend on both the vibrometer's noise floor and the amplitude of the acoustic field, and the spatial averaging uncertainty, which arises due to imperfect planarity across the active region of the hydrophone. The spatial averaging becomes increasingly restrictive at shorter wavelengths particularly in non-linearly steepened acoustic fields [24,25].

A key challenge in this approach is therefore finding a source of US that optimizes the calibratable frequency range by maximizing the acoustic amplitude over as wide a frequency range as possible. This should be conducted within the linear range of the interferometer whilst minimizing the spatial averaging uncertainty. There is considerable freedom in choosing this field, as vibrometers can be used to measure with any acoustic excitation, in particular in this context, they can measure tone-bursts, nonlinearly steepened tone-bursts, or pulses. One approach is to use a piezoelectric source to generate high amplitude tone-bursts that propagate nonlinearly through water generating a broad range of frequencies at the harmonics of the fundamental. By focusing the acoustic field, the pressure amplitude can be increased, which, as well as being beneficial to the SNR, also enhances the non-linear steepening leading to higher harmonics being present. This technique is currently exploited at PTB with their laser doppler vibrometer (LDV). They use a 50 mm focal length piezoelectric transducer centered at 7 MHz to calibrate hydrophones up to 100 MHz [17,26]. However, focusing increases the uncertainty related to spatial averaging (around 20% at 100 MHz) [17], as the focal spot size – the area over which the field is planar – becomes comparable in size to the active sensing area of the hydrophone. Not only does this limit the size of hydrophone that can be calibrated, but the measurement is sensitive to small positional offsets. Attempts to correct for the non-planarity of the field at the hydrophone either by numerical [24,27,28] or analytic inverse-filter [25,29] methods require some knowledge of the acoustic field at the measurement plane. Even so, there is a limit to the extent to which the uncertainty can be reduced using a correction approach, and it is clearly better to generate a plane wave acoustic field over the receive aperture of the hydrophone. Spatial averaging correction methods like these [6,24,25,27–29] are essential for accurate calibration of diagnostic and therapeutic transducers that intentionally produce focused

beams. However, calibration of hydrophones could be simplified if the source transducer produces waves that are nearly planar across the hydrophone sensitive element.

Ultrasound generation via the photoacoustic effect using a short duration optical pulse could be a promising alternative to piezoelectric transducer technology that has the potential to satisfy bandwidth, planarity, and high-amplitude requirements [30–32]. In photoacoustics, when a light absorbing medium is illuminated by an optical pulse, the photons are absorbed by chromophores in the medium and the subsequent thermalization of the energy leads to simultaneous increases in temperature and pressure within the absorption volume. If the medium is elastic and the energy deposition is sufficiently rapid, the pressure rise will result in an ultrasound pulse. Nanocomposites made of carbon nanoparticles dispersed in polymer matrices have been found to be strongly optically absorbing. Consequently, different types of carbon-based nanocomposites have been studied to generate Mega-Pascal range ultrasound pressure pulses for biomedical imaging and therapeutic applications [33–35].

In this paper, the design, fabrication, and characterization of a carbon-based laser-generated ultrasound (LGUS) source that generates a spatially broad, high-pressure, and broad bandwidth ultrasound pulse is described. The required characteristics of a calibration source which would enable hydrophone calibrations up to 100 MHz are listed in Section 2. The design and fabrication of the completed source is described in Section 3. The characteristics of the source such as its temporal stability, pulse-pressure and beam shape are detailed in Section 4. The systematic effects arising from implementing the source in a calibration configuration, such as the measurement repeatability and spatial averaging are discussed in Section 5.

2. Ideal characteristics of a calibration source

The aim of this work was to develop a state-of-the-art acoustic source for a hydrophone calibration system based on optical-interferometry. The source should have the following characteristics:

- i. The pressure-pulse should have a frequency range that makes measurements possible up to 100 MHz.
- ii. The spatial averaging of the ultrasound beam by the hydrophone for sensitive element diameters up to 600 μm should produce significantly lower uncertainties than current best practice (focused ultrasound fields) i.e., uncertainty should be less than 1% at all frequencies.
- iii. The temporal stability should be such that the amplitude of the LGUS pulses should vary by less than 2% from its mean over a three-hour test period, which is sufficient to calibrate at least one hydrophone using an interferometer.
- iv. The source must not contaminate the water, e.g., affect its conductivity.
- v. The source must not elevate the temperature of the water and thereby affect the sensitivity of the hydrophone.
- vi. The source must not present a hazard to the user.

A planar laser-generated ultrasound source using a carbon-polymer nanocomposite was proposed as a potential means of generating a field satisfying these requirements. A number of nanocomposite fabrication methods have been experimented with and reported in the literature for biomedical applications. This has been recently summarized in two review articles [33,34] and a book chapter [35]. A similar source has been used to characterize US sensor directional responses [36].

The source and its characterization are described in the subsequent sections.

3. Design and fabrication of the calibration source

3.1. Carbon-polymer nanocomposite source

The choice of the carbon-polymer nanocomposite (CPN) material was based on a previous study in which multi-walled carbon nanotubes (CNT) of three different weight percentages (1.25, 2.5 or 3.5 wt%) were dispersed mechanically in three different polymers (epoxy, polydimethylsiloxane (PDMS) or polyurethane (PU)) using a high-speed shear mixer [31,32]. The resulting CPN materials were coated on laboratory grade glass slides (0.8 mm thick, 26 mm wide, 76 mm length) using a manual micrometer-controlled blade film applicator of three thickness ranges (18–30, 40–60, or 50–70 μm). The 27 CPN sources were assessed as a function of CNT wt. %, polymer-type, coating thickness, laser fluence (10, 20, 30 and 40 mJcm^{-2}) and temporal stability under sustained laser excitation of 30 mJcm^{-2} over one hour. The laser wavelength was 1064 nm and the full-width at half-maximum pulse duration (FWHM) was 4 ns. Some of the key findings are briefly repeated here. Epoxy and PU-based CPN sources were found to be unsuitable due to the detachment of the CPN coating from the glass slide under sustained laser excitation and PDMS-based CPN sources were the most stable (and no detachment from glass) with a variation of less than 1% in the measured hydrophone voltage signals. For a fixed laser pulse duration and a given polymer-type, increasing the CNT wt. % did not increase the pressure amplitude. This is because the stress relaxation time, $\tau_{ac} = (\mu_a c_0)^{-1}$, decreases with optical absorption coefficient, μ_a [m^{-1}], where c_0 [m s^{-1}] is the sound-speed of the CPN material. If the laser pulse duration, τ , is not significantly shorter than τ_{ac} then the pressure wave starts to leave the heated region before the heating is completed, thereby limiting the magnitude of the acoustic pulse (also known as *stress confinement*) [37–39]. The CPN sources are typically more acoustically absorbing than the pure matrix material. Therefore, the thickness should ideally be equal to the optical absorption depth or as thin as practically achievable to minimize unnecessary acoustic absorption and loss of high frequencies. The peak-positive pressures from the PDMS-based CPN sources ranged from 2 to 7 MPa and were found to be nonlinearly dependent on the laser fluence. The -6 dB bandwidth metric scaled inversely proportionally to the peak pressure. This was caused by the steepening of the LGUS wavefront due to cumulative acoustic nonlinearity, which is a function of the medium nonlinearity, pressure amplitude, propagation distance and pulse shape [40]. The changing wave shape, coupled with stronger absorption of higher frequencies in water, resulted in loss of both amplitude and bandwidth as confirmed with measurements and modelling studies [31]. In order to minimize the losses, the source-hydrophone separation should be as small as practically achievable, which in our case was within 3–7 mm.

The CPN source element for the LGUS source was designed around a fused silica parallel disc of 5 ± 0.1 mm thickness and 50 mm diameter (FSW18, Newport Corporation, U.K.) on which the CPN layer was coated. The multi-walled CNT (Haydale Ltd., Ammanford, Carmarthenshire, U.K.) were mechanically dispersed in PDMS using a high-speed shear mixer (DAC 150.1 FV-K, SpeedMixerTM, High Wycombe, U.K.). As per the specifications from Haydale Ltd., the diameter and the length of individual CNT were 10 nm and 1.5 μm , respectively. Although the supplied multi-walled CNT were functionalized to contain carboxylic-acid (COOH) groups, the effect of functionalization on the quality of dispersion or fabrication was not studied independently. The CNT (240 mg corresponds to 2 wt%), PDMS (9.76 g), and catalyst (2 g) were all combined in a cylindrical plastic jar compatible with the shear mixer. The CNT were dispersed in the polymer at 3500 rotations per minute (rpm) for 2 min followed by addition of the catalyst, and shear mixed again at 3500 rpm for 2 min. A blade film applicator (Tefcom Microm II Film Applicator, Gardco, FL, USA) was used to coat the nanocomposite paste in which a height adjustable knife-edged metal frame attached to a pair of micrometers

controls the gap clearance relative to a flat surface, i.e., the glass disc. A thin film is produced when the excess mixture spread on the glass disc is removed by sliding the knife-edged metal frame over the surface of the glass disc. A glass-backed CPN source is formed after oven-curing the thin film at 100 °C for 30 mins [31]. A total of four source CPN source elements were fabricated. The average coating thickness was 20 μm with a standard deviation of 3 μm . The coating thickness of each source element was determined by measuring the uncoated glass and then the glass with the cured coating across six sites using a 1 μm resolution digital screw gauge.

3.2. Laser

The key laser specifications were for the pulse duration, fluence, and laser pulse delivery method. The laser pulse duration should ideally satisfy stress confinement i.e., $\tau \ll \tau_{ac}$ but due to the high optical absorption of the CPN sources across the visible and near infrared spectrum [31], a picosecond range duration laser would be required. For a 2.5 wt% CNT in PDMS, τ_{ac} is 5 ns, as calculated from μ_a and c_0 of pure PDMS in ref. [31]. Picosecond lasers with sufficient output energy are available but due to cost prohibitions a Q-switched laser (1064 nm) with FWHM duration below 4 ns was specified, which was considered sufficient. The acoustic beam close to the CPN source resembles the laser illumination area and therefore by increasing the illumination area a broad acoustic beam can be generated. In our previous work [31], a fluence of 20 mJcm^{-2} with an optical beam diameter of 10 mm (-20 dB) achieved via beam modifying optics and 4 ns FWHM duration produced peak-positive pressures of up to 5 MPa for a 2.5 wt% CNT in PDMS. In that case the source-hydrophone separation was 7.4 mm. This implies that for a 20 mm beam diameter, and keeping the same fluence, the required laser energy becomes 70 mJ. The laser type was chosen to be diode-pumped, rather than flash lamp-pumped, due to its compact size. Since the laser is of high energy and an open-beam delivery of the invisible wavelength laser poses a safety hazard to users, an optical fiber delivery system was specified. It was also desirable to obtain a trigger-out signal by placing a photodetector close to the exit aperture of the laser. This will enable synchronization with other hardware such as oscilloscope and automated scanning required for ultrasound field mapping. The M-Nano laser from Montfort GmbH (Götzis, Austria) closely matched these specifications. For the experiments, the laser module was mounted on a standard optical steel breadboard, which provided the necessary conductive cooling, with convective cooling achieved using a small cooling fan positioned close to the laser module. The temporal stability was monitored from cold switch-on of the laser – once with cooling fan on, once off – for one hour. After the first 20-min, the standard deviation for both measurements were typically 0.5%. The FWHM pulse duration was 2.6 ns, measured at the end of the fiber-bundle using an external high-speed photodetector (DET0CL, Thorlabs, Exeter, U.K.) and was comparable to that measured by the internal photodetector placed close to the exit aperture inside the laser system.

3.3. Design and fabrication of the source housing

A modular cylindrical housing was designed and fabricated to hold the nanocomposite source at one end, with a middle section to hold optical elements if required, for example to expand the laser beam, and with an adaptor at the opposite end to attach securely to an optical fiber-bundle. The entire aluminum assembly was designed to be water-tight. The Computer Aided Design (CAD) drawings and fabrication were carried out by NPL's Engineering team. The completed LGUS source is shown in Fig. 1. The source element is secured in a circular plastic frame with front screws for easy replacement in the event of damage to the coating surface. The inner diameter (50 mm) of the middle section was designed to hold standard optical components from Thorlabs, Inc. A 1500 grit ground glass optical diffuser was placed inside the middle section, which homogenized the laser beam and increased the



Fig. 1. Modular design of the LGUS source fabricated from aluminum. Clockwise: The CPN source element is securely held in a front plastic frame which is attached with screws to the middle section. The middle section holds a Thorlabs, Inc 1500 grit ground glass diffuser to both expand and homogenize the laser beam to a diameter of nearly 30 mm. The fiber-bundle is gripped by the two grub screws on the end section which in turn is secured to the middle section with screws.

illumination diameter to nearly 30 mm (measured approximately with a photosensitive card). The measured pulse energy after the diffuser was 43 mJ, which is the energy incident on the CPN.

4. Characterization of the calibration source

4.1. Measurement setup

The measurement setup used for source characterization is shown in Fig. 2. A 5-axis gantry with rotation and tilt, facilitated by a two-axis manual goniometer stage and three motorized linear axes (LNR50S/M, Thorlabs, Ely, U.K.) and controlled by dedicated scanning software (UMS2, Precision Acoustics Ltd., Dorchester, U.K.), was used for scanning the LGUS beam. A thermocouple placed inside the water tank was used to record the water temperature (not shown in Fig. 2). The laboratory operating conditions maintained the temperature of the water at 20 ± 1.0 °C. Three uncoated coplanar membrane type hydrophones from Precision Acoustics Ltd were employed for characterizing the LGUS beams of geometrical diameters 0.2 mm (UT1602), 0.4 mm (UT1604) and 0.6 mm (UT1606). The UT1604 hydrophone was calibrated from 1 to 60 MHz for its magnitude and phase response using a secondary calibration procedure [41,42]. The hydrophone response was also extrapolated from 60 to 110 MHz as described in ref. [31]

using a model of the hydrophone developed at NPL [43]. The pressure-time series were recovered from the measured UT1604 hydrophone voltage waveforms using deconvolution [6]. A Tektronix oscilloscope (DPO7254, Tektronix, Beaverton, OR, USA) was used to acquire the hydrophone waveforms, and the acquisition trigger to the oscilloscope was provided by the laser system. The waveforms were sampled at 1 GS/s and the waveform record consisted of 2000 data points.

4.2. Interfacial reflections

The acoustic pressure generated in the CPN will divide into two equal parts, one propagating to the left, $p_L(t)$, and the other to the right, $p_R(t)$. Consider the case in which the hydrophone is located in water to the left of the CPN source (Fig. 2). The two waves, when they arrive at the edge of the CPN source, are presented with CPN-glass and CPN-water interfaces respectively, where step changes in the acoustic impedance occur. The wave entering the water will therefore be the product of the initial wave and the CPN-water transmission coefficient, and the wave reflected at the CPN-glass interface will be multiplied by the CPN-glass reflection coefficient. It will then be transmitted into the water too, and subsequent reverberations within the CPN layer are possible (although they will become progressively damped). On a longer timescale, the right-going wave transmitted into the glass

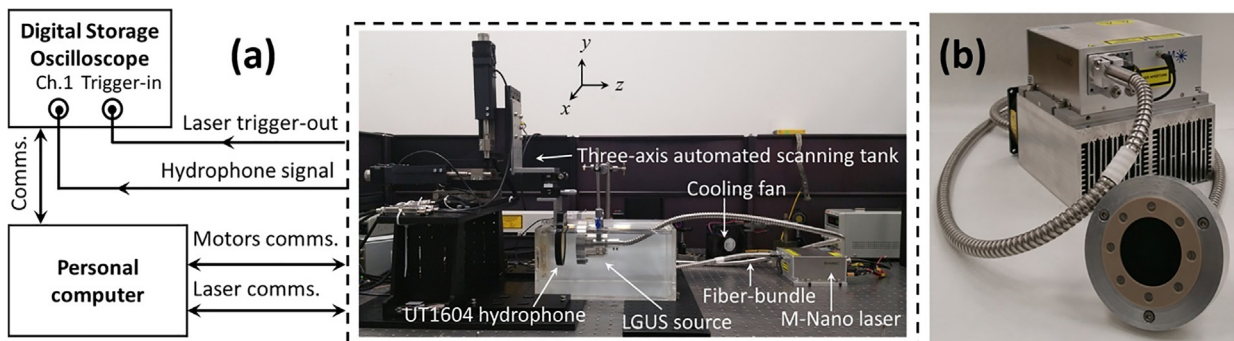


Fig.2. (a) Automated scanning tank set-up with fixed LGUS source and hydrophone mounted on the three-axis automated scanning tank. The tilt and rotation alignments of the hydrophone were aided by manual goniometer stages fitted to one of the linear stages. Axis convention: z – axis of propagation, y – vertical and x – horizontal. (b) Laser cooling arrangement using a fan-cooled heat sink. Two DC voltage driven axial fans are mounted on one end of the hollow fin aggregates (not visible in the picture).

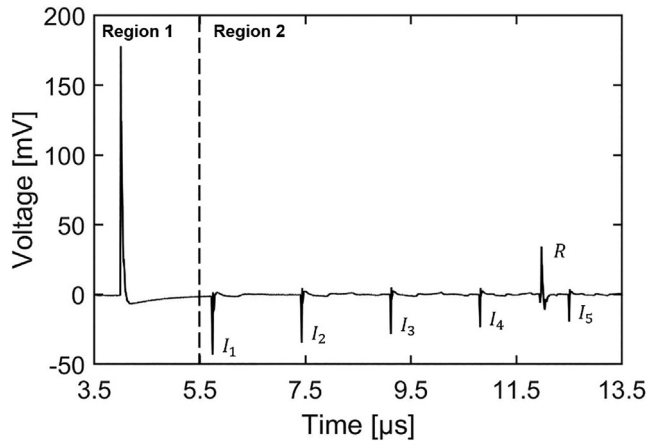


Fig. 3. The main LGUS pulse and the subsequent pulses due to internal reflections recorded using a membrane hydrophone. Region 1 corresponds to the initial transmitted pulse comprising of $p_L(t)$ and $p_R(t)$ first reflected at the CPN-glass interface. Region 2 contains the pulses due to internal reflections (annotated $I_1 - I_5$), which are time-gated out during calibration procedures. The polarity change in the trailing part of the pulse in Region 1 is due to diffraction arising from the Gaussian profile of the excitation laser beam. The positive pulse in Region 2 (annotated R) is the reflection of the main LGUS pulse from the hydrophone and then back from the source face.

backing will reflect from its rear and pass back through the CPN and into the water.

Fig. 3 is a voltage time-series acquired using a membrane hydrophone over a long acquisition window showing these interfacial reflections. The plot area is divided into two regions. Region 1 corresponds to the initial transmitted part of $p_L(t)$ through the CPN-water interface, initial $p_R(t)$ first reflected at the CPN-glass interface and then transmitted through the CPN-water interface, and its subsequent reflections at the CPN-water and CPN-glass interfaces. Since the thickness of the CPN source is only $20 \mu\text{m}$, these reflections internal to the CPN

source are indistinguishable. The pulses in Region 2 are those transmitted into the glass backing, reflected at the rear glass-air interface, and transmitted through the CPN layer into the water, arriving at the hydrophone after a round-trip travel time of $1.8 \mu\text{s}$. The amplitude progressively diminishes with subsequent round-trip reflections. Also seen in Region 2 is the pulse from Region 1 after it has reflected from both the hydrophone and back from the source face. For the calibration, the pulse in Region 1 is the only wave of interest and all the other pulses are time-gated out during the measurements.

The polarity change in the trailing part of the pulse in Region 1 is due to diffraction arising from the Gaussian profile of the excitation laser beam. (To understand this, consider the case of a laser beam with a top-hat profile incident on the CPN surface. In this case a sharp discontinuity in the absorbed energy density occurs, which gives rise to a boundary diffraction wave known as the edge-wave [44]. In case of Gaussian laser beam profile, such a distinct edge-wave is not generated but a negative wave is still present. The effect of laser beam profiles has been theoretically studied with experimental validation in ref. [45]).

4.3. Long-time temporal stability

A measure of the long-time temporal stability of the calibration source was obtained by measuring and analyzing the hydrophone voltage signals acquired for all four sources over three hours. This choice of time period reflects the length of time required to complete one hydrophone calibration on the Primary Standard. The UT1602 hydrophone was positioned at 5.5 mm from the source and aligned to the maximum of the LGUS beam at the measurement plane. The hydrophone voltage signal was averaged on the oscilloscope for eight trigger sweeps before saving each waveform. The stability was assessed by analyzing the peak-positive voltages of the waveform records acquired every three seconds over the three hours.

Each plot shown in **Fig. 4** is normalized to the beginning of the respective measurement data set. Firstly, there are rapid fluctuations of around 1% (except for Source #4) that can be ascribed to the small number of waveform averages used for these stability tests. During

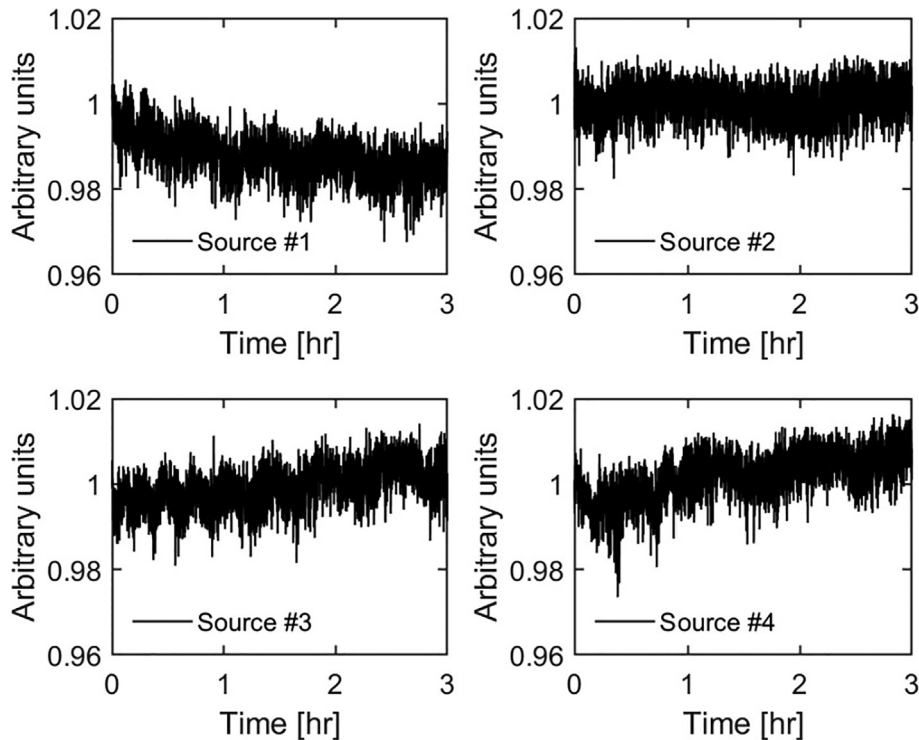


Fig. 4. Temporal stability plots of the four PDMS-based glass-backed CPN sources. Each data point in the plot is an average of eight sweep signals. Each plot was normalized to the beginning of the respective measurement data set.

calibrations normally 1000 waveform averages are performed and consequently these rapid fluctuations would be averaged out. Second, there is a slowly-varying fluctuation (except for Source #2), in which the source amplitude shows a gradual change of less than 2% from its mean over the three-hour test period. This variation is acceptable, and this is long enough for a typical calibration of a hydrophone, which involves up to six measurements repeated at 20-minute intervals. Any source that exhibits a variation of more than 2% in its mean output within the three-hour test period, then such a source could be rejected from use for example Source #4. Finally, it is also important to note that the CNT encapsulated in the polymer matrix did not contaminate the water, as confirmed by measuring the electrical conductivity of the water before and after the long-time temporal studies and confirming that it had not changed.

4.4. Source surface temperature

The sensitivity of hydrophones can change with temperature. The temperature-dependent sensitivity coefficient of the coplanar type PVDF membrane hydrophone over 1–10 MHz was measured as $0.65\% \text{ } ^\circ\text{C}^{-1}$ [22]. The optically-induced temperature rise within the LGUS source, which accompanies the acoustic pressure generation, diffuses into the cooler surroundings, which includes the region of water between the LGUS source and the hydrophone. Temperature measurements were taken on the surface of the LGUS source (Source #3) and on the active element of the hydrophone. A K-type thin-wire thermocouple connected to a data logger (USB-TC01, National Instruments, Austin, Texas, USA) was used for this purpose. The source-hydrophone separation was 5.5 mm. The surface temperature of the LGUS source increased by $3.3 \text{ } ^\circ\text{C}$ within 20 s from cold switch-on and remained stable thereafter. However, the temperature of the water in front of the hydrophone over one-hour period did not change from its ambient value of $19.8 \text{ } ^\circ\text{C}$. This suggested that the source surface temperature increase was not significant enough to cause the temperature of the water in front of the hydrophone to increase thereby not affecting the sensitivity of the hydrophone.

4.5. Time-series and spectra

A test measurement was obtained by applying the LGUS source on the UHF-120 model LDV from Polytec Ltd (Coventry, U.K.) on which the future primary hydrophone calibration standard at NPL is going to be based. The UHF-120 LDV has an analog bandwidth of 600 MHz and the optical beam diameter at a 500 mm stand-off distance is around $50 \text{ } \mu\text{m}$. A velocity pulse was measured by placing a pellicle (polyethylene terephthalate film of $5 \text{ } \mu\text{m}$ thickness with a gold coating of 25 nm on one side stretched on a 100 mm diameter annular ring) in front of the

LGUS source and the LDV beam was reflected from the gold-coated side of the pellicle. The velocity pulse shown in Fig. 5 has velocity components up to at least 100 MHz as shown in the corresponding magnitude spectra, which is very encouraging. The peak velocity of the pulse corresponds to a peak-positive pressure of 5.6 MPa at a source-pellicle separation of 7.4 mm. This was estimated using the following acoustic plane wave relation [46]

$$p = u\rho_0c_0, \quad (1)$$

where, p [Pa] is the acoustic pressure, u [ms^{-1}] is the acoustic particle velocity, ρ_0 [kgm^{-3}] and c_0 [ms^{-1}] are the temperature dependent ambient mass density and sound-speed of water, respectively.

The LDV measurements will be affected by the acousto-optic effect, which is the modulation of the optical refractive index as a result of the density changes in an acoustic wave. Here it is a potential concern because the LDV beam is arranged to pass through water in the NPL setup that will be carrying the US pulse, and the significance of the subsequent change in optical path-length needs to be assessed, as it will register as an addition to the velocity measured by the LDV [47]. The acousto-optic correction that is applied to pressure measurements from the LDV when using tone-burst ultrasound signals is negligibly small as they time-average to almost zero [48]. However, the LGUS pulse emerging from the CPN source is principally a positive pulse and therefore, there may be a small systematic effect on the measured velocity by the LDV. Future work will assess the effect of acousto-optic effect and if it is significant then an air-backed pellicle will be used. The use of air-backed pellicle will result in the doubling of measured velocity due to pressure-release boundary condition at the air and water interface, which will need to be taken into consideration, but it will remove the path of the LDV beam through the water and thus remove any potential for an acousto-optic effect error.

The measurements of the beam plots given in Section 4.6, were performed using a hydrophone, since it was not possible to scan the LDV with its current set-up. A set of voltage time-series acquired from the UT1604 hydrophone and their corresponding magnitude spectra are shown in Fig. 6. The hydrophone response was deconvolved from the time-series using the procedure described in ref. [31]. The resulting LGUS pressure-pulses and their corresponding magnitude spectra are shown in Fig. 5. The peak-positive pressures from the four source elements measured at a source-hydrophone separation of 5.5 mm ranged from 7.3 to 8.4 MPa. It should be borne in mind that the deconvolved pressure-pulses are affected by the bandwidth of the hydrophone, the frequency range over which the hydrophone is calibrated, and the planarity of the acoustic beam. Frequency response deconvolution has been studied widely in the literature [9,29,42,49–52].

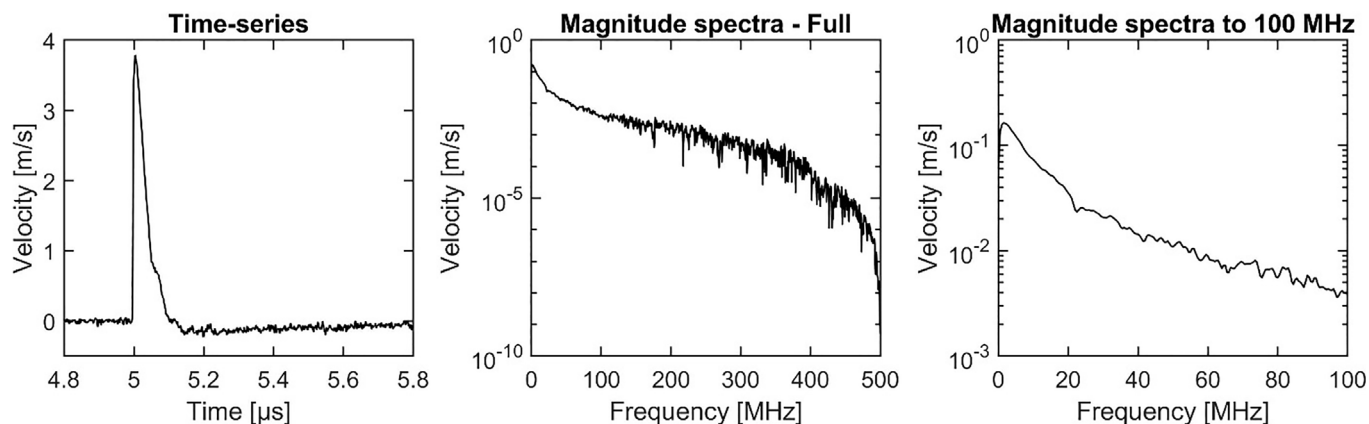


Fig. 5. The velocity pulse corresponds to Source #3, which was measured by reflecting the LDV (UHF-120, Polytec Ltd.) beam from a pellicle. The calculated magnitude spectra show velocity components at least up to 100 MHz.

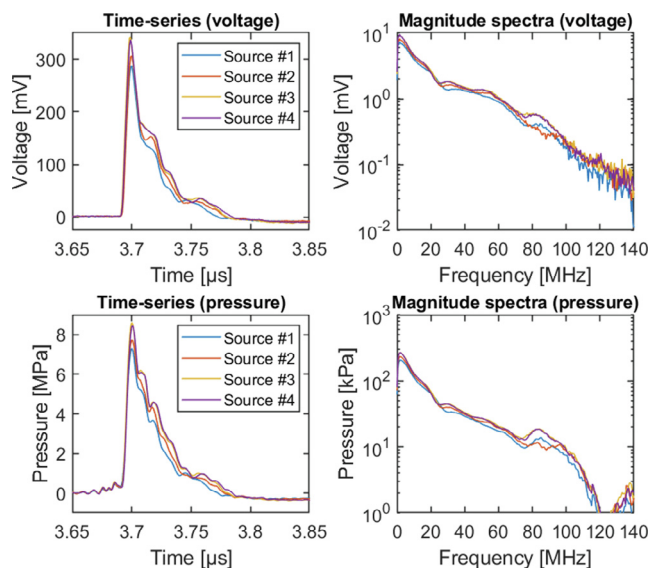


Fig. 6. Top row: Voltage time-series acquired from UT1604 hydrophone and their corresponding magnitude spectra from all four source elements. Bottom row: Pressure time-series were recovered from the measured hydrophone voltage waveforms via deconvolution.

4.6. Beam scans

Beam scans were performed to measure the spatial profile of the LGUS beam, and to estimate the laser fluence, since the laser beam will have the same profile. Three separate scans were performed using the UT1604 hydrophone in the x - y , x - z , and y - z planes. The scan step size was 0.25 mm, and the source-hydrophone separation was 5.2 mm. Fig. 7 shows the beam scans for Source #3. (Beam scans from the three other sources were comparable.) The FWHM of the beam in x - y plane was around 8 mm. The beam-area was estimated by summing the areas of all the pixels at which the beam energy was greater than or equal to 10% (or -20 dB) of the peak value in the raster scan image. The average beam-area from the scans of the four sources in the x - y plane was 3.19 ± 0.08 cm². The pulse energy after the diffuser was 43 mJ, which gives an average fluence of 13.5 mJcm⁻² on the surface of the CPN.

5. Considerations in the use of the calibration source in a primary standard

5.1. Measurement repeatability

The long-time temporal stability has already been discussed in Section 4.3. Here the impact of the temporal stability on measurement repeatability is assessed in a secondary hydrophone calibration scenario using 0.2 mm, 0.4 mm, and 0.6 mm diameter membrane hydrophones.

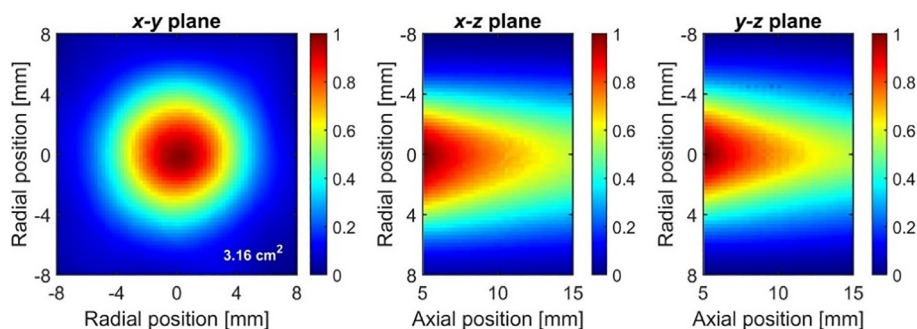


Fig. 7. Beam scans of the LGUS field from Source #3 in x - y , x - z and y - z planes obtained using the UT1604 membrane hydrophone. The scan step size was 0.25 mm. The peak hydrophone voltages recorded from the raster scan were rescaled between (0, 1) for each measurement plane.

The 0.2 mm diameter hydrophone was a Precision Acoustics D1202 type since the UT1602 type hydrophone was not available at the time of this particular study. The PVDF film thickness of D1202 is nominally 12 μ m and has a differential input amplifier. Additionally, the average magnitude sensitivity of the D1202 hydrophone from 1 to 60 MHz is a factor of 2.6 higher than UT1604 and 1.5 higher than UT1606 hydrophones. The measurement repeatability was assessed by statistically analyzing the quality of spectral (magnitude) ratios for a pair of hydrophones from repeat measurement data sets. For this purpose, the hydrophone signals were measured in the LGUS beam of Source #1 at a source-hydrophone separation of 5 μ s via time-of-flight (or ~ 7.4 mm). The alignment of the hydrophone to the maximum of the beam in the measurement plane was achieved by a combination of line scan measurements in x - and y -axes and manual angular adjustments. Once the alignment process was completed, a hydrophone signal was acquired, and the process was repeated using the other two hydrophones. A total of six repeat measurements were performed on each hydrophone.

The standard errors or the Type A uncertainties [53] in the measurement were evaluated on the magnitude ratios from six repeat measurements for a pair of hydrophones i.e., 0.4 mm over 0.2 mm, 0.6 mm over 0.2 mm, and 0.6 mm over 0.4 mm. The Type A uncertainties shown in Fig. 8 are equivalent or better to those derived using piezoelectric transducers up to the overlapping frequency of 60 MHz in primary hydrophone calibration procedures. The Type A uncertainties in the magnitude calibration of a membrane-type hydrophone at 60 MHz on NPL and PTB setups are 7.5% and 2.08%, respectively [17,22]. Overall, the Type A uncertainties seen in Fig. 8 are acceptably low, which confirms that the trend observed in long-time temporal stability (see Fig. 4) of the LGUS sources is not a concern during calibrations on the Primary Standard.

5.2. Spatial averaging errors

The pressure measured by the hydrophone is, to a first approximation, an average of the acoustic field incident on the surface of the finite-sized active element. If the incident pressure amplitude is not uniform across the active element, then spatial averaging will result in a measured amplitude lower than the peak pressure and, crucially, different from the pressure measured by the LDV due to its superior spatial resolution. The beam profile of the LGUS beam shown in Fig. 7 is Gaussian, not planar. Consequently, the pressure will not be uniform over the surface of the hydrophone, introducing a spatial averaging error in the measurement. The larger the active element of the hydrophone the greater the error. Therefore, the significance of the error due to spatial averaging in the LGUS beam was assessed for three membrane hydrophones of 0.2 mm, 0.4 mm and 0.6 mm diameters.

An empirical model previously developed at NPL was used to calculate the spatial averaging corrections (inverse of the error) for the three hydrophone sizes [54]. The method requires following two frequency dependent parameters to be known to calculate the required

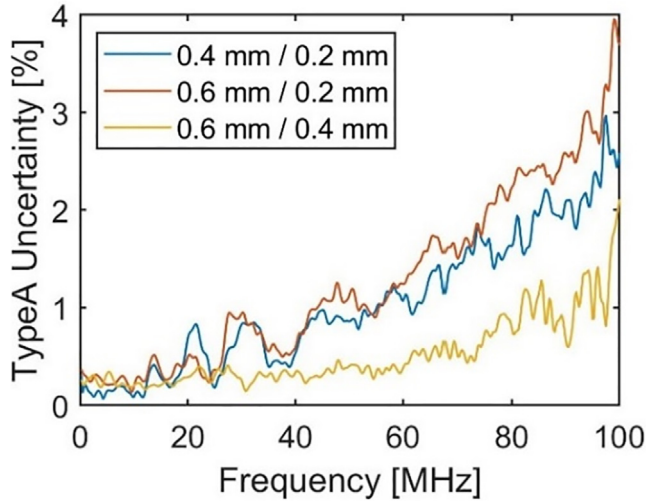


Fig. 8. Type A measurement uncertainty calculated from the spectral (magnitude) ratios for a pair of 0.2 mm, 0.4 mm, and 0.6 mm diameter membrane hydrophones over six independent repeat measurements in the LGUS beam of Source #1.

corrections i) the directional response of the hydrophone from which the effective diameter, $d_{\text{eff}}(f)$ is calculated [28,55] and ii) the -6 dB beam-width measured at the measurement plane using the spectra of the hydrophone voltage pulse. The directional response for the three hydrophones was not measured but the nominal effective hydrophone diameters were obtained using the empirical relationship [28,56]

$$d_{\text{eff}}(f) = 2 \times \sqrt{a_g^2 + \frac{1}{4f^2}}, \quad (2)$$

where, a_g is the nominal geometrical radius and f is the frequency in MHz. It is worth noting that there are alternate functional forms for membrane hydrophones that have also been successful in modelling $d_{\text{eff}}(f)$ [57,58].

The spatial averaging correction, δ , is derived using the empirical relationship

$$\delta(f) = 1 + \frac{0.3}{([\text{beamwidth}(f)/d_{\text{eff}}(f)]^2 + 0.3)}. \quad (3)$$

The effective hydrophone diameters, $d_{\text{eff}}(f)$, calculated using Eq. (2) for 0.2 mm, 0.4 mm, and 0.6 mm diameter hydrophones, are shown in Fig. 9. Also, shown in the same figure are the measured -6 dB beam-widths through the beam maximum at a source-hydrophone separation

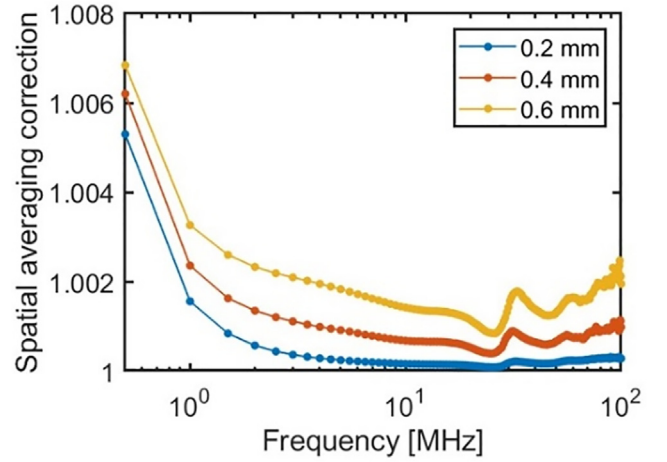


Fig. 10. Spatial averaging corrections for 0.2 mm, 0.4 mm and 0.6 mm diameter membrane hydrophones calculated using Eq. (3). The corrections were calculated from the average of the frequency dependent beam-widths measured in x and y -axes at a source-hydrophone separation of 5.2 mm in the LGUS beam of Source #3. The effective hydrophone diameters for the three membrane hydrophones were calculated using Eq. (2).

of 5.2 mm, which corresponds to the LGUS beam of Source #3. The frequency dependent beam-widths were obtained from the magnitude spectra of each hydrophone voltage waveform recorded from the line scan along the x and y -axes. The y -axis corresponds to the long electrode axis of the hydrophone. The features seen in the beam-width plots are discussed in the subsequent paragraph. The calculated spatial averaging corrections for the three hydrophones are shown in Fig. 10. The corrections are below 1% at all frequencies and hence the uncertainty contribution will be negligible during calibrations for hydrophone diameters up to 0.6 mm. In comparison, the correction for a 0.5 mm diameter membrane hydrophone was 3.4% at 60 MHz in a nonlinearly steepened field generated by a 5 MHz focused transducer [21].

The prominent structures seen in the beam-width plots, which appear consistently at the same frequencies for different hydrophones is likely to have arisen from the interfacial reflections that are part of the main pulse as described in Section 4.2. This can be experimentally investigated by using a LGUS source either with twice or half the CPN layer thickness used in this study (nominally 20 μm) in which case the constructive and destructive interfacial reflections should occur at different frequencies. Also, the beam-widths of the 0.2 mm hydrophone

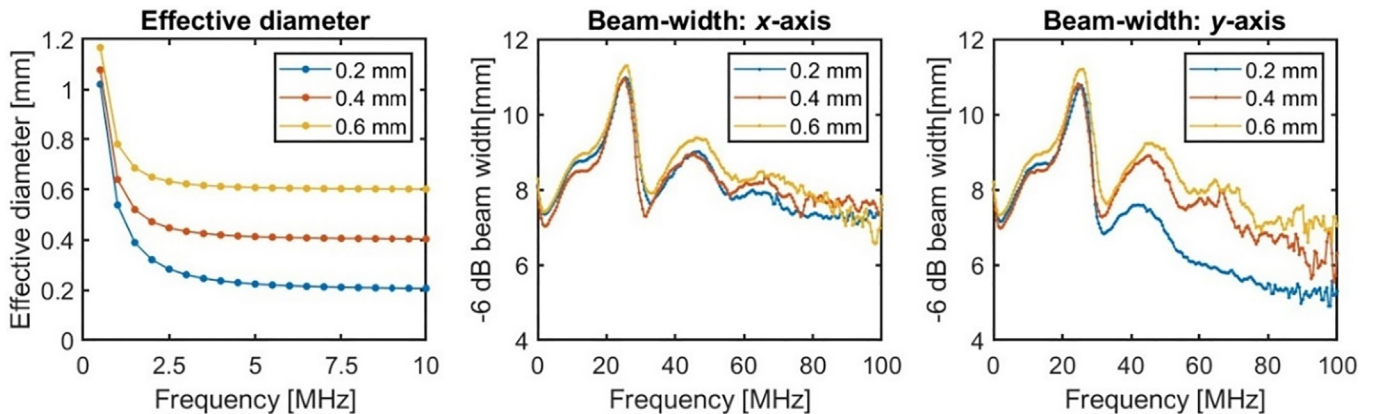


Fig. 9. Effective diameters calculated using Eq. (2) for 0.2 mm, 0.4 mm, and 0.6 mm diameter membrane hydrophones. The effective diameters are plotted only up to a frequency of 10 MHz since the values converge to the nominal geometrical values beyond 10 MHz. The frequency dependent beam-widths were obtained from the magnitude spectra of each hydrophone voltage waveform recorded along the line scans along the x and y -axes at the position of the beam maximum. The source-hydrophone separation was 5.2 mm and measurement data correspond to the LGUS beam of Source #3.

were consistently found, in repeated measurements, to be lower in the y -axis compared to the 0.4 mm and 0.6 mm hydrophones. The exact reasons were not investigated, but possibly this could be due to asymmetry in the geometrical dimensions of the sensing element.

Finally, it is important to emphasize that there are other approaches to calculating spatial averaging corrections i.e., numerical [24,27,28] and analytic inverse-filter [25,29] methods. The method used above provides a representative range of corrections for theoretical membrane hydrophone diameters given that $d_{\text{eff}}(f)$ was not measured. This approach was deemed sufficient for the purpose of this study. However, when calibrating hydrophones on the Primary Standard, $d_{\text{eff}}(f)$ will be determined from experimentally measured directional response data as prescribed in the standard IEC 62127-3 [55].

6. Conclusions

In this paper, the design and fabrication of a high-pressure, broadband, plane-wave, laser-generated ultrasound calibration source has been described. Its characteristics were measured, including the peak pressure amplitude (several MPa), bandwidth (> 100 MHz), beam profile (full-width and half maximum), and long-time temporal stability (better than 2% variation from mean). The uncertainties arising from the use of the LGUS source in a calibration scenario were assessed, including the measurement repeatability and effect of spatial averaging. These were equivalent or better than those achieved in existing hydrophone calibration procedures using piezoelectric transducers.

All tests conducted on the LGUS source indicate its suitability for hydrophone calibrations up to 100 MHz. It is anticipated that future Primary Standard calibrations employing LGUS sources in combination with LDV detectors will significantly lower uncertainties in comparison to current procedures.

Declaration of Competing Interest

The authors declare that they have no known competing financial interests or personal relationships that could have appeared to influence the work reported in this paper.

Acknowledgements

S.R. thanks the U.K. Department for Business, Energy & Industrial Strategy's funding of the National Measurement System and NPL for funding his PhD with University College London. The authors also thank Dr Bajram Zeqiri, Dr Toby Sainsbury, Dr Chris Fury, colleagues of Ultrasound and Underwater Acoustics Group, Engineering Services team of NPL, Dr Bradley Treeby, and UCL's Biomedical Ultrasound Group. B.T.C. acknowledges the European Union's Horizon 2020 research and innovation program H2020 ICT 2016-2017 under Grant agreement No. 732411, which is an initiative of the Photonics Public Private Partnership.

References

- [1] Z. Izadifar, P. Babyn, D. Chapman, Mechanical and Biological Effects of Ultrasound: A Review of Present Knowledge, *Ultrason. Med. Biol.* 43 (2017) 1085–1104, <https://doi.org/10.1016/j.ultrasmedbio.2017.01.023>.
- [2] G. Ter Haar, Ultrasound bioeffects and safety, *Proc. Inst. Mech. Eng. Part H J. Eng. Med.* 224 (2010) 363–373, <https://doi.org/10.1243/09544119JEM613>.
- [3] A. Fomenko, C. Neudorfer, R.F. Dallapiazza, S.K. Kalia, A.M. Lozano, Low-intensity ultrasound neuromodulation: An overview of mechanisms and emerging human applications, *Brain Stimul.* 11 (2018) 1209–1217, <https://doi.org/10.1016/j.brs.2018.08.013>.
- [4] K.K. Shung, High Frequency Ultrasonic Imaging, *J. Med. Ultrasound.* 17 (2009) 25–30, [https://doi.org/10.1016/S0929-6441\(09\)60012-6](https://doi.org/10.1016/S0929-6441(09)60012-6).
- [5] M.S. Canney, M.R. Bailey, L.A. Crum, V.A. Khokhlova, O.A. Sapozhnikov, Acoustic characterization of high intensity focused ultrasound fields: A combined measurement and modeling approach, *J. Acoust. Soc. Am.* 124 (2008) 2406–2420, <https://doi.org/10.1121/1.2967836>.
- [6] IEC 62127-1:2007 + AMD1:2013, Amendment 1—Ultrasonics—
- [7] P. Morris, A. Hurrell, A. Shaw, E. Zhang, P. Beard, A. Fabry-Pérot fiber-optic ultrasonic hydrophone for the simultaneous measurement of temperature and acoustic pressure, *J. Acoust. Soc. Am.* 125 (2009) 3611–3622, <https://doi.org/10.1121/1.3117437>.
- [8] S.M. Howard, Calibration of reflectance-based fiber-optic hydrophones, *IEEE Int. Ultrason. Symp. IUS. 2016-Novem* (2016) 2–5. doi:10.1109/ULTSYM.2016.7728572.
- [9] V. Wilkens, S. Sonntag, O. Georg, Robust spot-poled membrane hydrophones for measurement of large amplitude pressure waveforms generated by high intensity therapeutic ultrasonic transducers, *J. Acoust. Soc. Am.* 139 (2016) 1319–1332, <https://doi.org/10.1121/1.4944693>.
- [10] E. Martin, E.Z. Zhang, J.A. Guggenheim, P.C. Beard, B.E. Treeby, Rapid Spatial Mapping of Focused Ultrasound Fields Using a Planar Fabry-Pérot Sensor, *IEEE Trans. Ultrason. Ferroelectr. Freq. Control.* 64 (2017) 1711–1722, <https://doi.org/10.1109/TUFFC.2017.2748886>.
- [11] IEC 62359:2010/AMD1:2017, Amendment 1 - Ultrasonics - Field characterization - Test methods for the determination of thermal and mechanical indices related to medical diagnostic ultrasonic fields, International Electrotechnical Commission, Geneva, Switzerland, 2017.
- [12] IEC 60601-2-62:2013, Medical electrical equipment - Part 2-62: Particular requirements for the basic safety and essential performance of high intensity therapeutic ultrasound (HITU) equipment, International Electrotechnical Commission, Geneva, Switzerland, 2015.
- [13] IEC 60601-2-37:2007 + AMD1:2015 CSV, Medical electrical equipment - Part 2-37: Particular requirements for the basic safety and essential performance of ultrasonic medical diagnostic and monitoring equipment, International Electrotechnical Commission, Geneva, Switzerland, 2015.
- [14] S.M. Nagle, M.K. Moore, G. Sundar, M.E. Schafer, G.R. Harris, S. Vaezy, J.M. Gessert, S.M. Howard, R.M. Eaton, Challenges and regulatory considerations in the acoustic measurement of high-frequency (> 20 MHz) ultrasound, *J. Ultrasound Med.* 32 (2013) 1897–1911, <https://doi.org/10.7863/ultra.32.11.1897>.
- [15] N. Chris Chaggares, O. Ivanytskyy, Guofeng Pang, Design of a 30 μm aperture membrane hydrophone for the measurement and characterization of High Frequency ultrasound, in: 2016 IEEE Int. Ultrason. Symp., IEEE, 2016: pp. 1–6. doi:10.1109/ULTSYM.2016.7728861.
- [16] E. Jafarzadeh, A.N. Sinclair, Non-linear Wave Propagation and Safety Standards for Diagnostic Ultrasound Devices, *Ultrason. Med. Biol.* 45 (2019) 11–20, <https://doi.org/10.1016/j.ultrasmedbio.2018.08.021>.
- [17] M. Weber, V. Wilkens, Using a heterodyne vibrometer in combination with pulse excitation for primary calibration of ultrasonic hydrophones in amplitude and phase, *Metrologia.* 54 (2017) 432–444, <https://doi.org/10.1088/1681-7575/aa72ba>.
- [18] IEC 62127-2:2007 + AMD1:2013 + AMD2:2017 CSV, Ultrasonics - Hydrophones - Part 2: Calibration for ultrasonic fields up to 40 MHz, International Electrotechnical Commission, Geneva, Switzerland, 2017.
- [19] S. Rajagopal, C.R. Fury, B. Zeqiri, M. Brandt, V. Wilkens, C. Koch, Y. Matsuda, M. Yoshioka, Y. Ping, Z. Yan, B. Wenping, R.P.B. Costa-Felix, E.G. Oliveira, Report on BIPM/CIPM key comparison CCAUV.U-K4: absolute calibration of medical hydrophones in the frequency range 0.5 MHz to 20 MHz, *Metrologia.* 53 (2016), <https://doi.org/10.1088/0026-1394/53/1A/09004> 09004 09004.
- [20] D.R. Bacon, Primary Calibration of Ultrasonic Hydrophones Using Optical Interferometry, *IEEE Trans. Ultrason. Ferroelectr. Freq. Control.* 35 (1988) 152–161, <https://doi.org/10.1109/58.4165>.
- [21] T.J. Esward, S.P. Robinson, Extending the frequency range of the National Physical Laboratory primary standard laser interferometer for hydrophone calibrations to 60 MHz, *IEEE Trans. Ultrason. Ferroelectr. Freq. Control.* 46 (1999) 737–744, <https://doi.org/10.1109/58.764860>.
- [22] R.C. Preston, S.P. Robinson, B. Zeqiri, T.J. Esward, P.N. Gélat, N.D. Lee, Primary calibration of membrane hydrophones in the frequency range 0.5 MHz to 60 MHz, *Metrologia.* 36 (1999) 331–343. doi:10.1088/0026-1394/36/4/13.
- [23] S. Rajagopal, B. Zeqiri, P. Gélat, Calibration of miniature medical ultrasonic hydrophones for frequencies in the range 100 to 500 kHz using an ultrasonically absorbing waveguide, *IEEE Trans. Ultrason. Ferroelectr. Freq. Control.* 61 (2014) 765–778, <https://doi.org/10.1109/TUFFC.2014.2969>.
- [24] B. Zeqiri, A.D. Bond, The influence of waveform distortion on hydrophone spatial-averaging corrections—Theory and measurement, *J. Acoust. Soc. Am.* 92 (1992) 1809–1821, <https://doi.org/10.1121/1.403837>.
- [25] K.A. Wear, S.M. Howard, Correction for Spatial Averaging Artifacts in Hydrophone Measurements of High-Intensity Therapeutic Ultrasound: An Inverse Filter Approach, *IEEE Trans. Ultrason. Ferroelectr. Freq. Control.* 66 (2019) 1453–1464, <https://doi.org/10.1109/tuffc.2019.2924351>.
- [26] V. Wilkens, S. Sonntag, M. Weber, Secondary Complex-valued Hydrophone Calibration up to 100 MHz Using Broadband Pulse Excitation and a Reference Membrane Hydrophone, in: 2019 IEEE Int. Ultrason. Symp., IEEE, 2019: pp. 1846–1849. doi:10.1109/ULTSYM.2019.8926180.
- [27] M.P. Cooling, V.F. Humphrey, V. Wilkens, Hydrophone area-averaging correction factors in nonlinearly generated ultrasonic beams, *J. Phys. Conf. Ser.* 279 (2011), <https://doi.org/10.1088/1742-6596/279/1/012002>.
- [28] E.G. Radulescu, P.A. Lewin, A. Nowicki, W.A. Berger, Hydrophones' effective diameter measurements as a quasi-continuous function of frequency, *Ultrasonics.* 41 (2003) 635–641, [https://doi.org/10.1016/S0041-624X\(03\)00180-X](https://doi.org/10.1016/S0041-624X(03)00180-X).
- [29] K.A. Wear, Considerations for Choosing Sensitive Element Size for Needle and Fiber-Optic Hydrophones I: Spatiotemporal Transfer Function and Graphical Guide,

- IEEE Trans. Ultrason. Ferroelectr. Freq. Control. 66 (2019) 318–339, <https://doi.org/10.1109/TUFFC.2018.2886067>.
- [30] S. Rajagopal, T. Sainsbury, B.E. Treeby, B.T. Cox, Laser generated ultrasound sources using polymer nanocomposites for high frequency metrology, IEEE Int. Ultrason. Symp. IUS. (2017) 3–6, <https://doi.org/10.1109/ULTSYM.2017.8092019>.
- [31] S. Rajagopal, T. Sainsbury, B.E. Treeby, B.T. Cox, Laser generated ultrasound sources using carbon-polymer nanocomposites for high frequency metrology, J. Acoust. Soc. Am. 144 (2018) 584–597, <https://doi.org/10.1121/1.5048413>.
- [32] S. Rajagopal, B.E. Treeby, B.T. Cox, Effect of Backing on Carbon-Polymer Nanocomposite Sources for Laser Generation of Broadband Ultrasound Pulses, in: 2018 IEEE Int. Ultrason. Symp., IEEE, 2018: pp. 1–4. doi:10.1109/ULTSYM.2018.8579784.
- [33] S.-L. Chen, Review of Laser-Generated Ultrasound Transmitters and Their Applications to All-Optical Ultrasound Transducers and Imaging, Appl. Sci. 7 (2016) 25, <https://doi.org/10.3390/app7010025>.
- [34] S. Noimark, R.J. Colchester, R.K. Poduval, E. Maneas, E.J. Alles, T. Zhao, E.Z. Zhang, M. Ashworth, E. Tsolaki, A.H. Chester, N. Latif, S. Bertazzo, A.L. David, S. Ourselin, P.C. Beard, I.P. Parkin, I. Papakonstantinou, A.E. Desjardins, Polydimethylsiloxane Composites for Optical Ultrasound Generation and Multimodality Imaging, Adv. Funct. Mater. 28 (2018) 1–16, <https://doi.org/10.1002/adfm.201704919>.
- [35] T. Lee, H.W. Baac, Q. Li, L.J. Guo, Efficient Photoacoustic Conversion in Optical Nanomaterials and Composites, Adv. Opt. Mater. 6 (2018) 1800491, <https://doi.org/10.1002/adom.201800491>.
- [36] J.A. Guggenheim, E.Z. Zhang, P.C. Beard, A Method for Measuring the Directional Response of Ultrasound Receivers in the Range 0.3–80 MHz Using a Laser-Generated, Ultrasound Source, IEEE Trans. Ultrason. Ferroelectr. Freq. Control. 64 (2017) 1857–1863, <https://doi.org/10.1109/TUFFC.2017.2758173>.
- [37] G. Paltauf, P.E. Dyer, Photomechanical processes and effects in ablation, Chem. Rev. 103 (2003) 487–518, <https://doi.org/10.1021/cr010436c>.
- [38] A. Vogel, V. Venugopalan, Mechanisms of Pulsed Laser Ablation of Biological Tissues, Chem. Rev. 103 (2003) 577–644, <https://doi.org/10.1021/cr010379n>.
- [39] T.J. Allen, B.T. Cox, P.C. Beard, Generating photoacoustic signals using high-peak power pulsed laser diodes, in: Photons Plus Ultrasound Imaging Sens. 2005, 2005: pp. 233–242. doi:10.1117/12.597321.
- [40] T.L. Szabo, Nonlinear Acoustics and Imaging, in: Diagnostic Ultrasound Imaging Insid. Out, Elsevier, 2004: p. 576.
- [41] R.A. Smith, D.R. Bacon, A multiple-frequency hydrophone calibration technique, J. Acoust. Soc. Am. 87 (1990) 2231–2243, <https://doi.org/10.1121/1.399191>.
- [42] A.M. Hurrell, S. Rajagopal, The Practicalities of Obtaining and Using Hydrophone Calibration Data to Derive Pressure Waveforms, IEEE Trans. Ultrason. Ferroelectr. Freq. Control. 64 (2017) 126–140, <https://doi.org/10.1109/TUFFC.2016.2594770>.
- [43] P.N. Gélat, R.C. Preston, A. Hurrell, A theoretical model describing the transfer characteristics of a membrane hydrophone and validation, Ultrasonics. 43 (2005) 331–341, <https://doi.org/10.1016/j.ultras.2004.08.003>.
- [44] M. Frenz, G. Paltauf, H. Schmidt-Kloiber, Laser-generated cavitation in absorbing liquid induced by acoustic diffraction, Phys. Rev. Lett. 76 (1996) 3546–3549, <https://doi.org/10.1103/PhysRevLett.76.3546>.
- [45] B.T. Cox, J.G. Lauffer, K.P. Kostli, P.C. Beard, Experimental validation of photoacoustic k-space propagation models, in: A.A. Oraevsky, L. V. Wang (Eds.), Photons Plus Ultrasound Imaging Sens., 2004: pp. 238–248. doi:10.1117/12.531178.
- [46] A.D. Pierce, Acoustics, in: 3rd ed., Springer International Publishing, 2019: p. 768. doi:10.1007/978-3-030-11214-1.
- [47] M. Cooling, V. Humphrey, P. Theobald, S. Robinson, The Influence of the Acousto-Optic Effect on LDV Measurements of Underwater Transducer Vibration and Resultant Field Predictions, in: 4th Int. Conf. Exhib. Underw. Acoust. Meas. Technol. Results, 2011: p. 619.
- [48] D.R. Bacon, Report EUR 10910 EN - The improvement and evaluation of a laser interferometer for the absolute measurement of ultrasonic displacements in the frequency range up to 15 MHz, 1985. <https://op.europa.eu/en/publication-detail/-/publication/d1b12b3d-40b6-4fe1-921f-7c1dc542feb2>.
- [49] K.A. Wear, P.M. Gammell, S. Maruvada, Y. Liu, G.R. Harris, Improved measurement of acoustic output using complex deconvolution of hydrophone sensitivity, IEEE Trans. Ultrason. Ferroelectr. Freq. Control. 61 (2014) 62–75, <https://doi.org/10.1109/TUFFC.2014.6689776>.
- [50] K. Wear, Y. Liu, P. Gammell, S. Maruvada, G. Harris, Correction for frequency-dependent hydrophone response to nonlinear pressure waves using complex deconvolution and rarefactional filtering: Application with fiber optic hydrophones, IEEE Trans. Ultrason. Ferroelectr. Freq. Control. 62 (2015) 152–164, <https://doi.org/10.1109/TUFFC.2014.006578>.
- [51] S. Eichstädt, V. Wilkens, A. Dienstfrey, P. Hale, B. Hughes, C. Jarvis, On challenges in the uncertainty evaluation for time-dependent measurements, Metrologia. 53 (2016) S125–S135, <https://doi.org/10.1088/0026-1394/53/4/S125>.
- [52] S. Eichstädt, V. Wilkens, Evaluation of uncertainty for regularized deconvolution: A case study in hydrophone measurements, J. Acoust. Soc. Am. 141 (2017) 4155–4167, <https://doi.org/10.1121/1.4983827>.
- [53] M3003, The Expression of Uncertainty and Confidence in Measurement, 4th ed., United Kingdom Accreditation Service, Staines-upon-Thames, 2019. <https://www.ukas.com/download/publications/publications-relating-to-laboratory-accreditation/M3003-Expression-of-Uncertainty-and-Confidence-in-Measurement-Edition-4-October-2019.pdf>.
- [54] R.A. Smith, Are hydrophones of diameter 0.5 mm small enough to characterise diagnostic ultrasound equipment? Phys. Med. Biol. 34 (1989) 1593–1607, <https://doi.org/10.1088/0031-9155/34/11/007>.
- [55] IEC 62127-3:2007 + AMD1:2013 CSV, Ultrasonics - Hydrophones - Part 3: Properties of hydrophones for ultrasonic fields up to 40 MHz, International Electrotechnical Commission, Geneva, Switzerland, 2013.
- [56] R.C. Preston, ed., Output Measurements for Medical Ultrasound, Springer, London, 1991. doi:10.1007/978-1-4471-1883-1.
- [57] V. Wilkens, W. Molkenstruck, Broadband PVDF membrane hydrophone for comparisons of hydrophone calibration methods up to 140 MHz, IEEE Trans. Ultrason. Ferroelectr. Freq. Control. 54 (2007) 1784–1791, <https://doi.org/10.1109/TUFFC.2007.462>.
- [58] K.A. Wear, C. Baker, P. Miloro, Directivity and Frequency-Dependent Effective Sensitive Element Size of Membrane Hydrophones: Theory Versus Experiment, IEEE Trans. Ultrason. Ferroelectr. Freq. Control. 66 (2019) 1723–1730, <https://doi.org/10.1109/TUFFC.2019.2930042>.